Supplementary information: Piezoresistive structural composites reinforced by carbon nanotube-grafted quartz fibres

H.G. De Luca[a], D.B. Anthony[b, c], E.S. Greenhalgh[c], A. Bismarck[d], and M.S.P. Shaffer[a, b*]

[a] Department of Materials, Imperial College London, London, United Kingdom
[b] Department of Chemistry, Imperial College London, London, United Kingdom
[c] Department of Aeronautics, Imperial College London, London, United Kingdom
[d] Institute of Materials Chemistry, Faculty of Chemistry, University of Vienna, Währinger Str. 42, 1090 Vienna, Austria

* Corresponding author (m.shaffer@imperial.ac.uk)

Table of Contents

S1 Quartz fibre tows and thermal gravimetric analysis

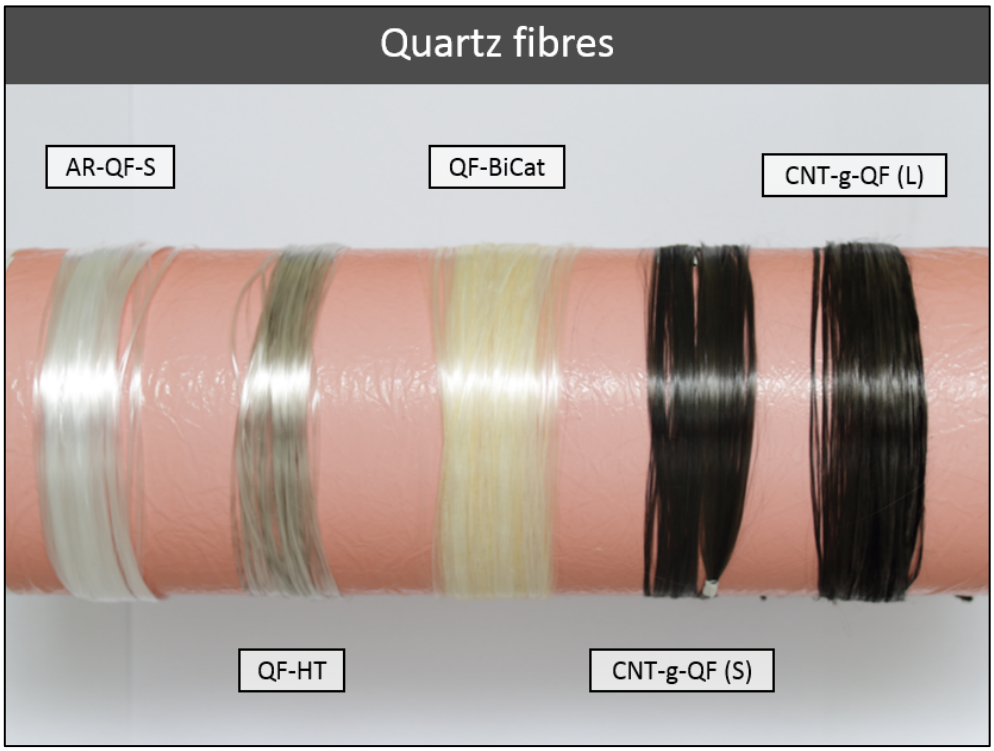

Fig. S1. Photograph of quartz fibres tow sections (two meter long) after different chemical and/or thermal treatment conditions (left to right: as-received, heat-treated, bi-catalyst decorated, short CNT grafted, long CNT grafted). The catalyst precursor deposition was performed on as-received sized quartz fibres.

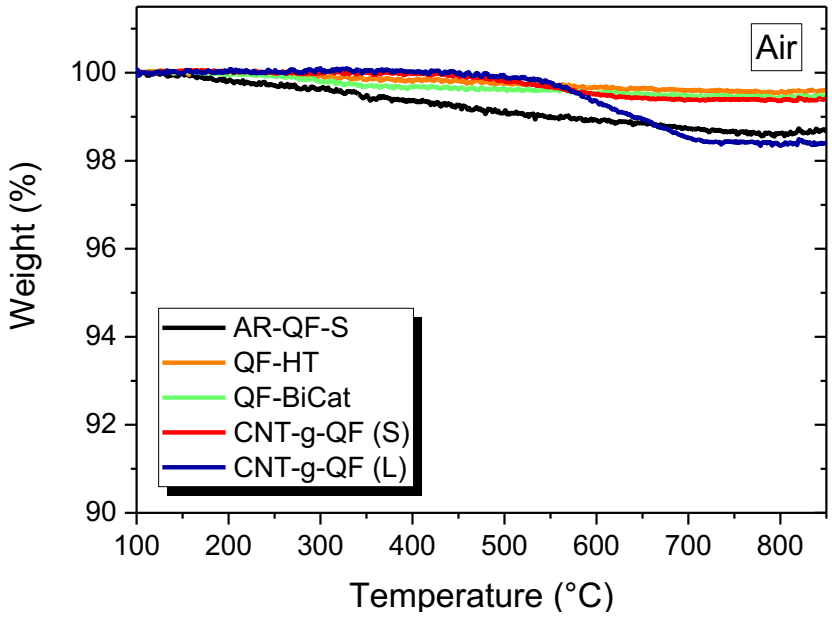

Fig. S2. TGA curves of as-received sized, heat-treated (thermally desized), bi-catalyst decorated and CNT-grafted quartz fibres with different growth duration; 12 min (S) and 24 min (L), respectively.

S2 Additional Raman spectra analysis

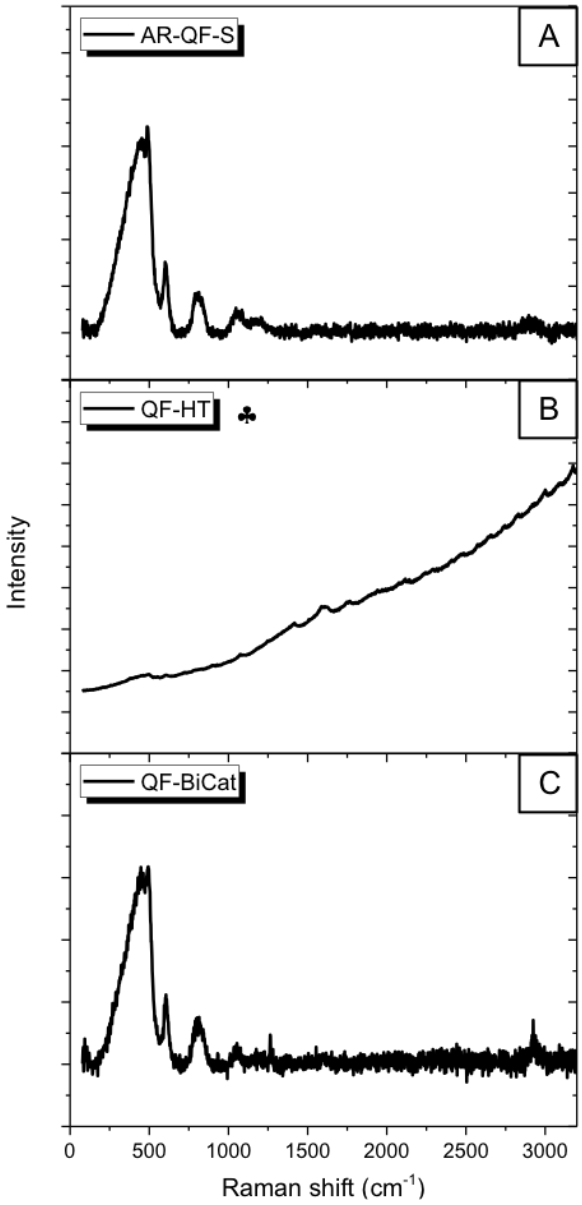

Fig. S3. Raman spectra for (a) as-received sized, (b) heat-treated (thermally desized) and (c) bi-catalyst decorated quartz fibres. ♣ Baseline for QF-HT was not subtracted due to the absence of peaks resulting in significant noise.

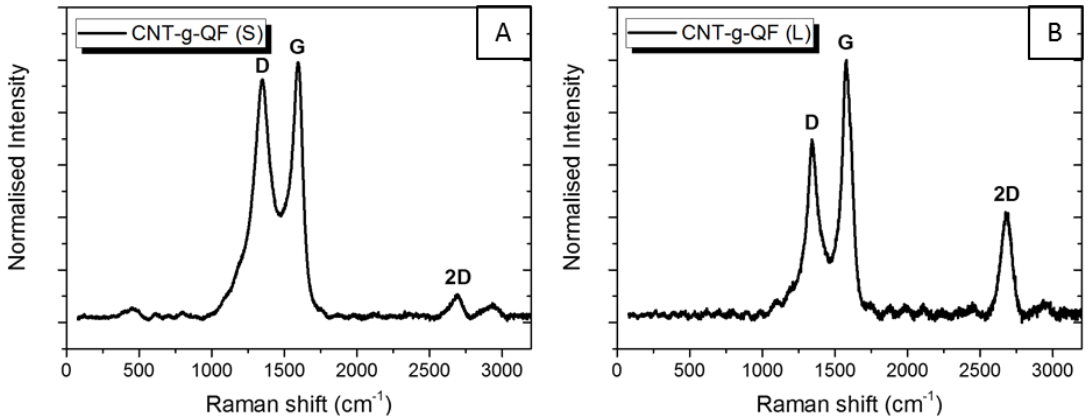

Fig. S4. Raman spectra of (a) CNT-g-QF (S) and (b) CNT-g-QF (L) after single fibre pull-out, away from the fracture surfaces with D-mode (1350 cm^{-1}), G-mode (1582 cm^{-1}) and 2D-mode (2700 cm^{-1}).

S3 Single fibre tensile test

Single fibre tensile test results (**Fig. S5**) show that the Young's modulus, a core fibre property, remains unaltered whilst tensile strength significantly decreases upon exposure to high temperatures (ca. 760 °C) for 30 min, in agreement with the tabulated mechanical data obtained from bundle composites (**Table S2**).

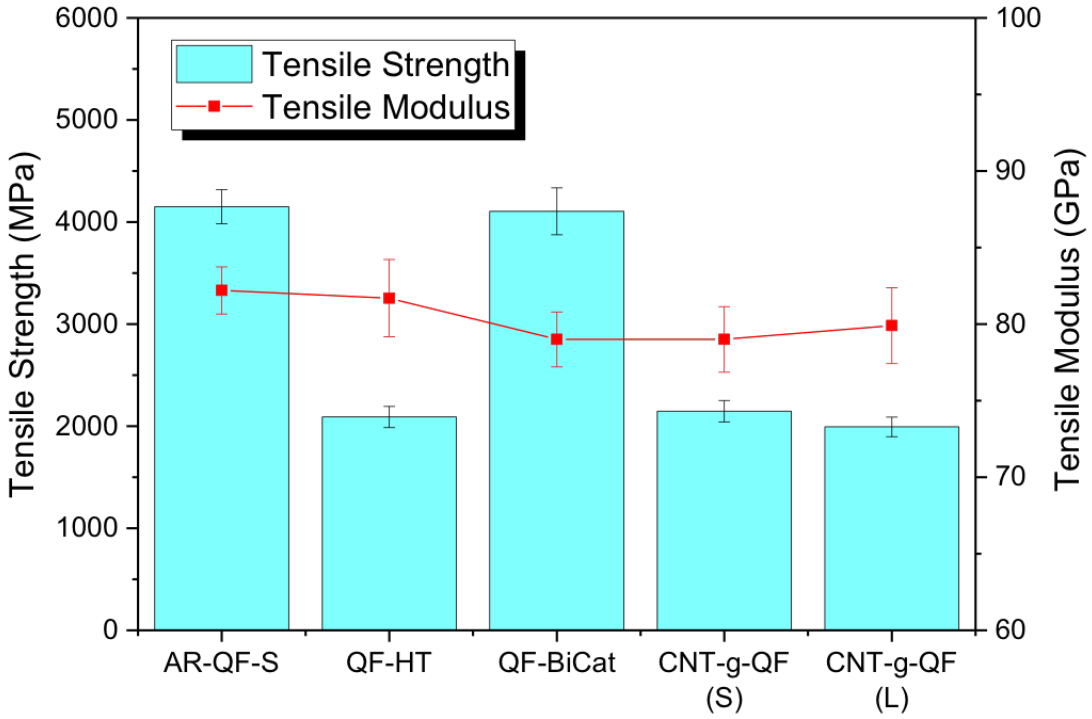

Fig. S5. Tensile properties of as-received quartz fibres before and after all thermal and/or chemical treatments, measured with a gauge length of 25 mm. Error bars correspond to standard error.

Table S1. Tabulated single fibre tensile properties measured with a gauge length of 25 mm with standard error associated.

	Tensile Strength (GPa)	**Tensile modulus** (GPa)	**# of spec.**
AR-QF-S	4.15 ± 0.17	82.2 ± 1.5	16
QF-HT	2.09 ± 0.10	81.7 ± 2.5	14
QF-BiCat	4.11 ± 0.23	79.0 ± 1.8	17
CNT-g-QF (S)	2.15 ± 0.10	79.0 ± 2.1	13
CNT-g-QF (L)	1.99 ± 0.10	79.9 ± 2.5	14

S4 Electrical conductivity anisotropy of the hierarchical bundles

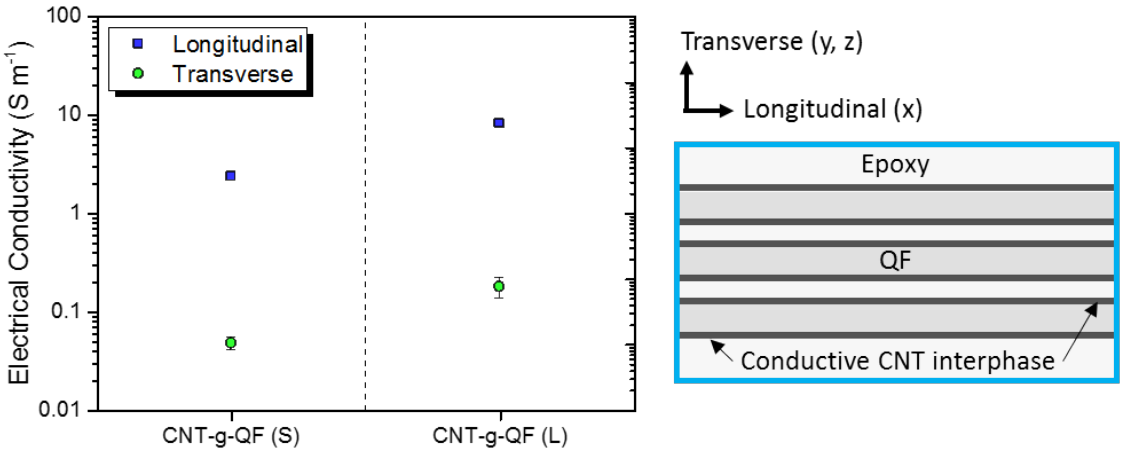

Fig. S6. *Ex-situ* electrical conductivity of the UD hierarchical bundle composites (longitudinal and transverse directions in relation to the loading direction) with standard error associated.

From the TGA analysis presented in **Fig. S2**, the CNT loading was estimated to be around 0.6 and 1.6 wt.% for CNT-g-QF (S) and CNT-g-QF (L), respectively, and around 0.3 and 0.6 wt.% for their respective hierarchical bundle composites. The high electrical conductivity measured for these relatively low CNT loadings is the result of an efficient CNT network formation at the fibre/matrix interface. For the short and uniform CNT coverage (i.e. CNT-g-QF (S)), the CNT volume fraction in the interphase region can be estimated as follows (**Eq. S1**). First, assuming a MWCNT density of 1.8 g cm^{-3} [1] and a quartz fibre density of 2.2 g cm^{-3} [2], we obtain a CNT volume fraction for CNT-g-QF (S) of ca. 0.74 vol.%, from:

$$v_{CNT\ (interphase)} = \frac{V_{CNT}}{V_{Interphase}} = \frac{0.0074 \times \pi R^2 \times 1\ u.l.}{\pi(R^2 - r^2) \times 1\ u.l.} \quad \text{(S1)}$$

where R is the radius of the CNT-g-QF (S), including the contribution from the 200 nm thick CNT layer, r the radius of the as-received QFs and u.l. corresponds to a unit length (**Fig. S7**). The geometric calculations suggest a CNT volume fraction of 12.6 vol.% within the interphase, consistent with aligned arrays of CNTs grown over large areas [3]. The CNT loading in the interphase region is approximately an order of magnitude higher than conventional percolation threshold in randomly distributed CNT/epoxy systems thus explaining the high electrical conductivity obtained in the fibre direction (**Fig. S6**). For the longer CNTs (i.e. CNT-g-QF (L)), the local density in the interphase region is

expected to be similar to that of the shorter, non-aligned CNTs (CNT-g-QF (S)). However, the CNT splayed "Mohawk" morphology, which leads to an apparently uneven CNT length along the tow, makes it difficult to estimate the CNT volume fraction more accurately.

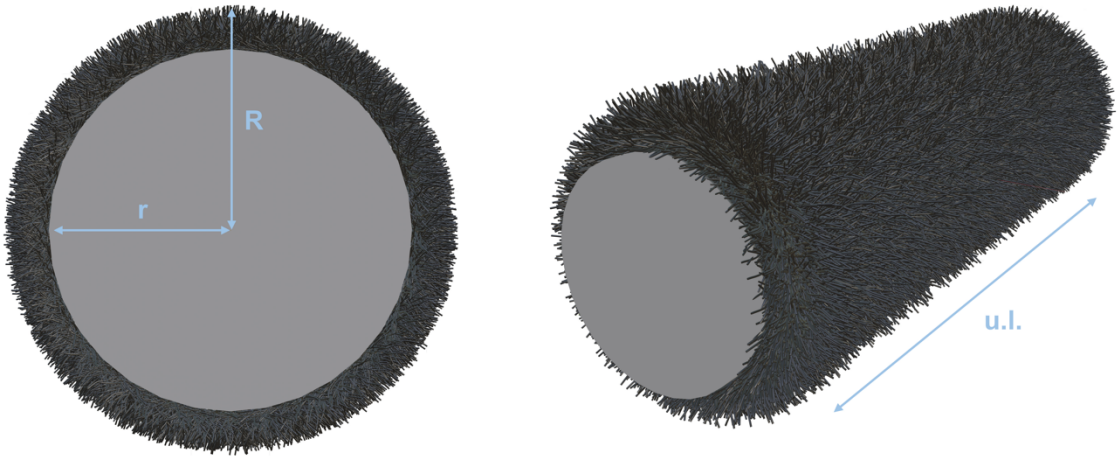

Fig. S7. A 3D model of a quartz fibre with a homogeneous coverage of short CNTs.

S5 Unidirectional hierarchical bundle composites acoustic emission

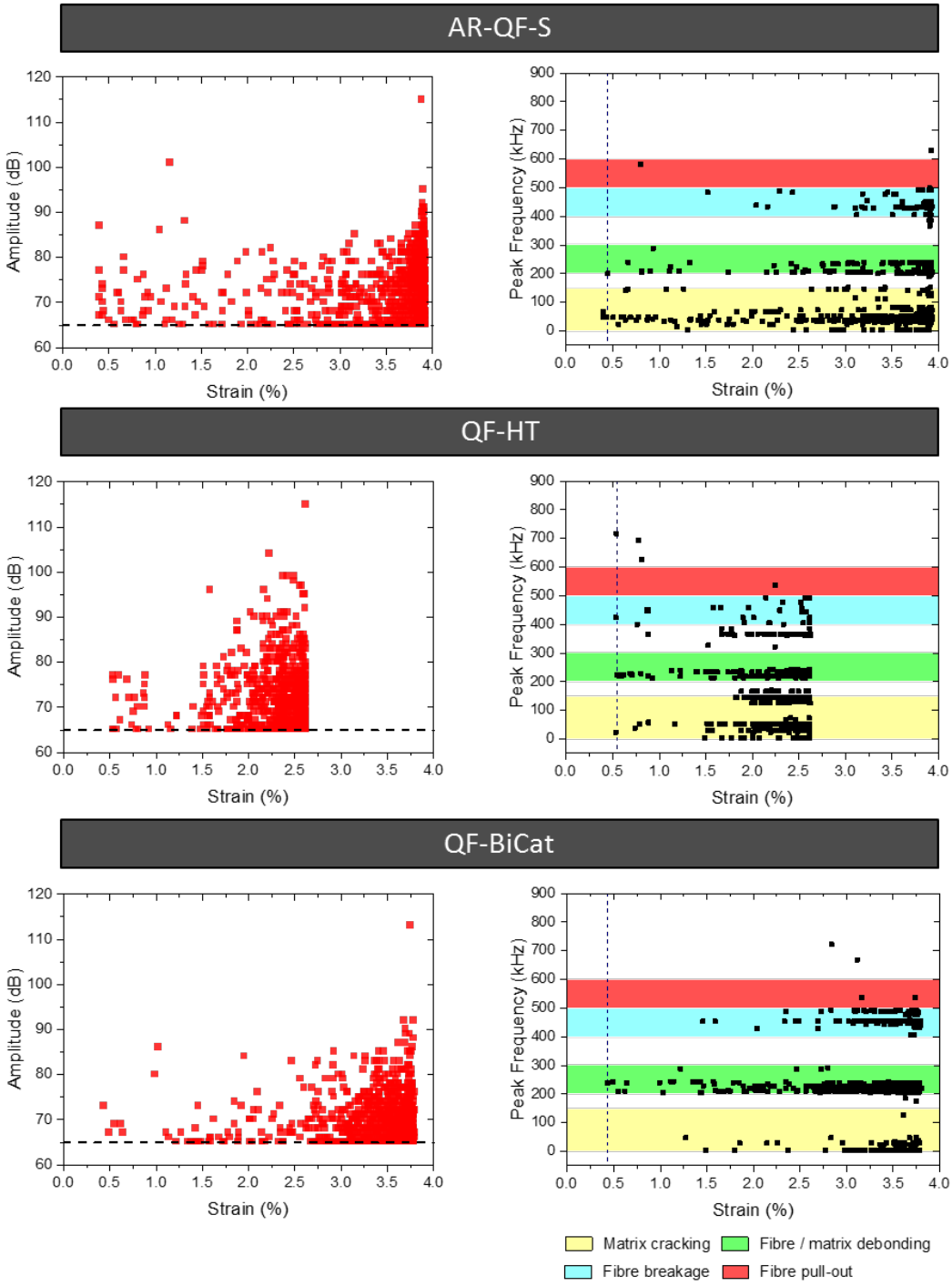

Fig. S8. Signal amplitude (left column) and peak frequency (right column) from acoustic emission events measured for all bundle composites (AR-QF-S, QF-HT, QF-BiCat, CNT-g-QF (S) and CNT-g-QF (L)) during tensile testing, and associated resistance-change ($\Delta R/R_0$) for UD hierarchical bundles. Vertical and horizontal dashed line correspond to 65 dB threshold and the onset of fibre/matrix debonding, respectively. Coloured peak frequency ranges were obtained from [4]. 0 – 150 kHz (yellow): matrix cracking; 200 – 300 kHz (green): fibre/matrix debonding; 400 – 500 kHz (blue): fibre failure; 500 – 600 kHz (red): fibre pull-out.

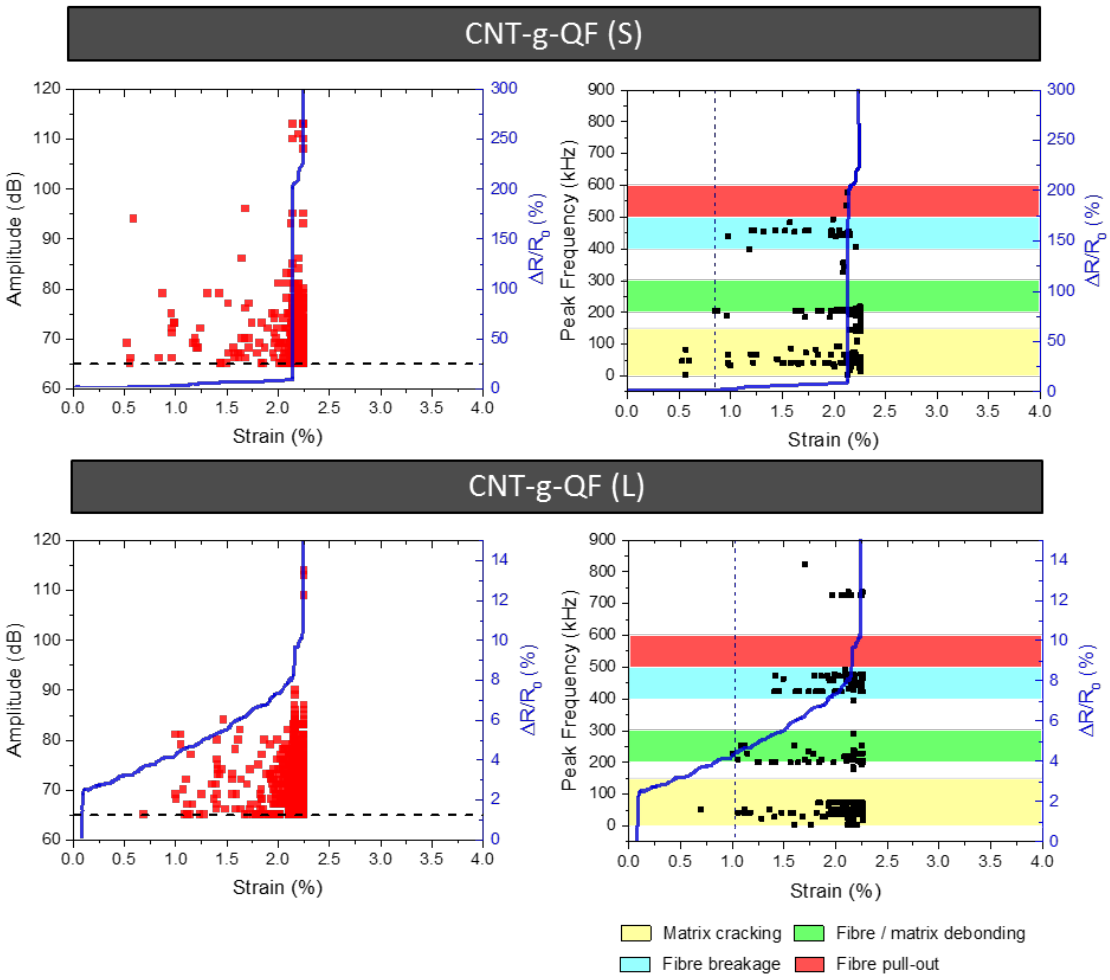

Fig. S8. (Continued).

S6 Additional micrographs

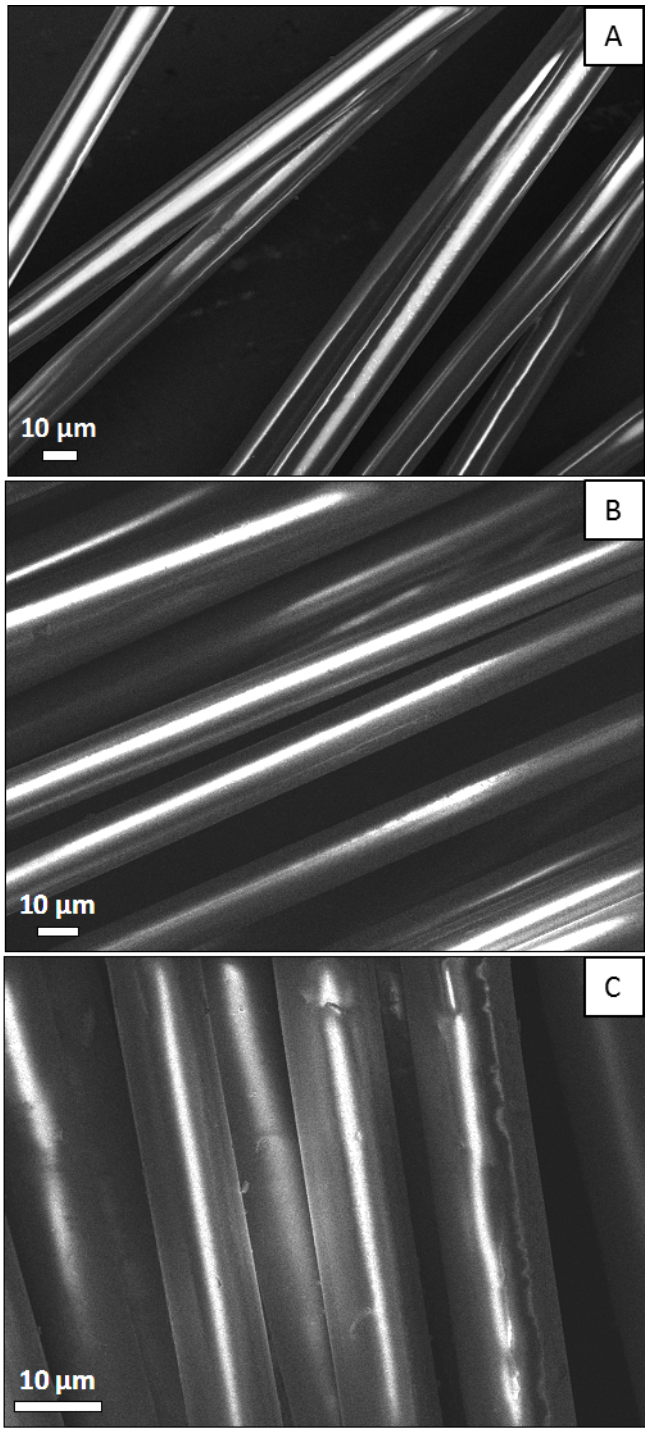

Fig. S9. FE-SEM micrographs of (a) as-received sized, (b) heat-treated (thermally desized) and (c) bi-catalyst decorated quartz fibres.

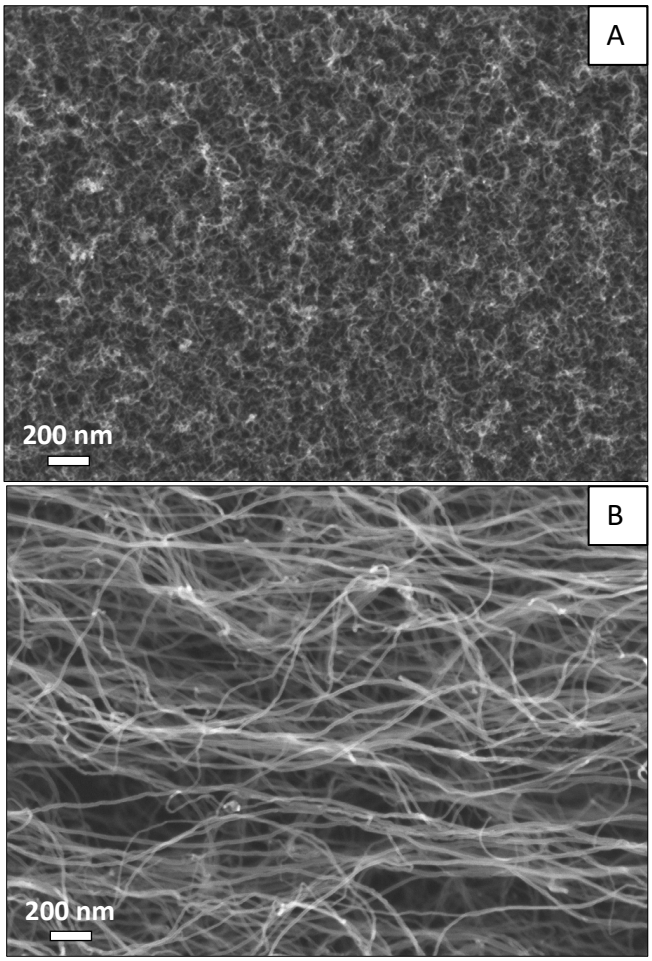

Fig. S10. High-magnification FE-SEM micrographs of (a) CNT-g-QF (S) and (b) CNT-g-QF (L). The shorter CNTs can only be easily viewed 'end on', whilst the Mohawk arrangement of the longer CNTs facilitates a transverse view.

S7 Unidirectional bundle composite set-up

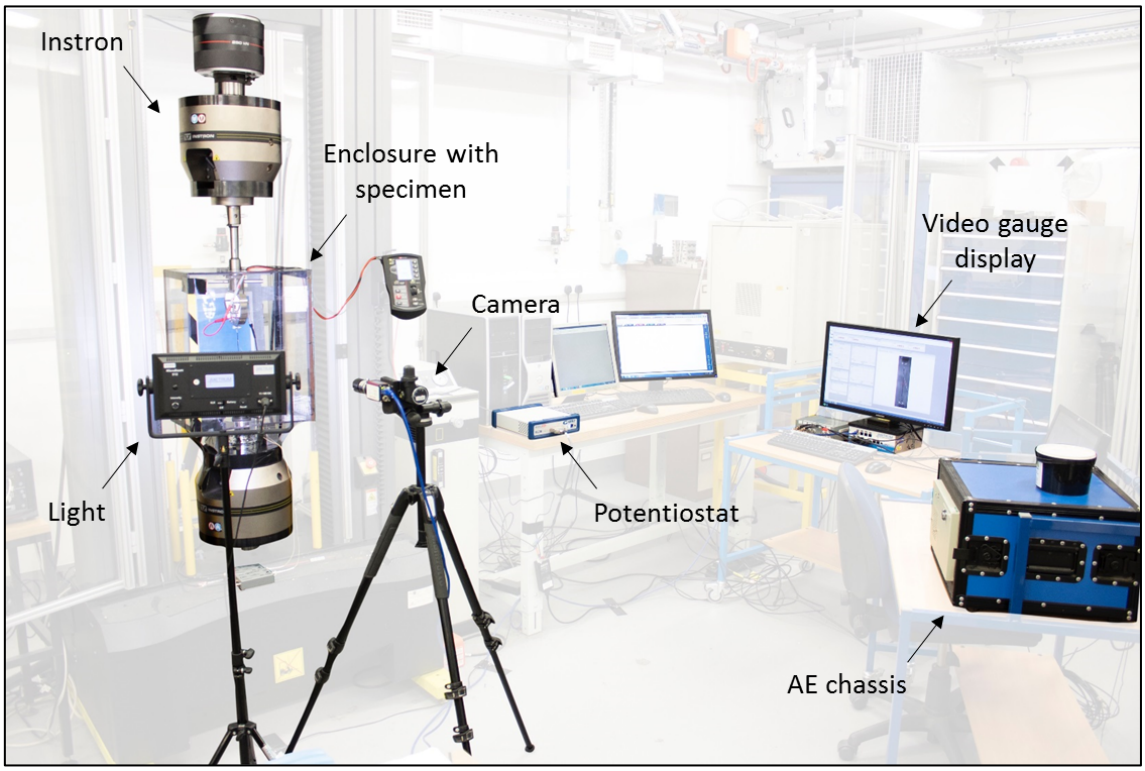

Fig. S11. Photograph of the bundle composite tensile test set-up with *in-situ* AE and electrical conductivity measurement. The video gauge camera and associated software records the pixel displacement from two painted marks on the sample surface. The sample is illuminated using a light source to ensure a suitable contrast for the video gauge software to track the points accurately. The force and displacement outputs from the Instron were also recorded *in-situ* with the strain measurements to ensure simultaneous data acquisition via an analogue to digital converter. In conjunction with these recordings acoustic emission events were detected though sensors placed on the sample's surface and processed by the AE chassis and associated software. Similarly, a fixed voltage was applied to the sample, in the loading direction, and the current recorded using a potentiostat to evaluate strain-dependent resistivity.

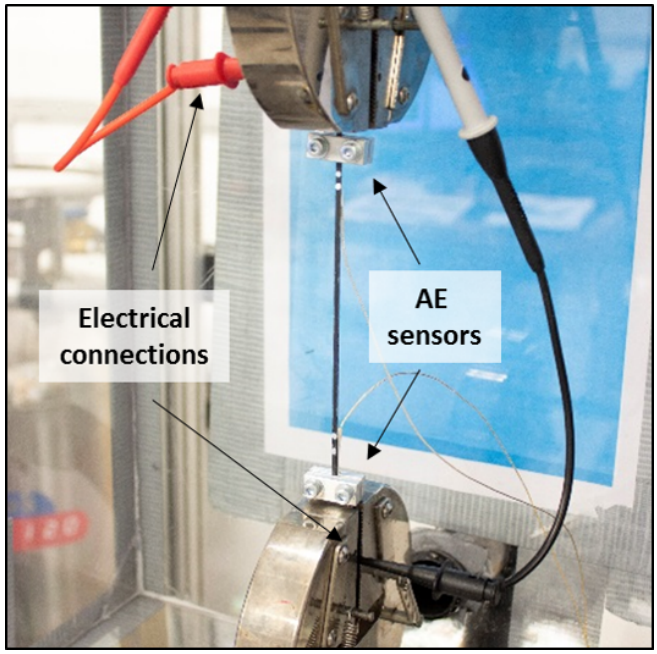

Fig. S12. Photograph of a hierarchical bundle composite under tensile loading (in the enclosure) with *in-situ* electrical conductivity and AE detection. AE sensors were clamped to the specimen using purpose-built aluminum jigs. Painted marks for the video gauge tracking were made close to the clamps situated at each end of the sample.

S8 Additional data from the tensile testing of the unidirectional bundle composites

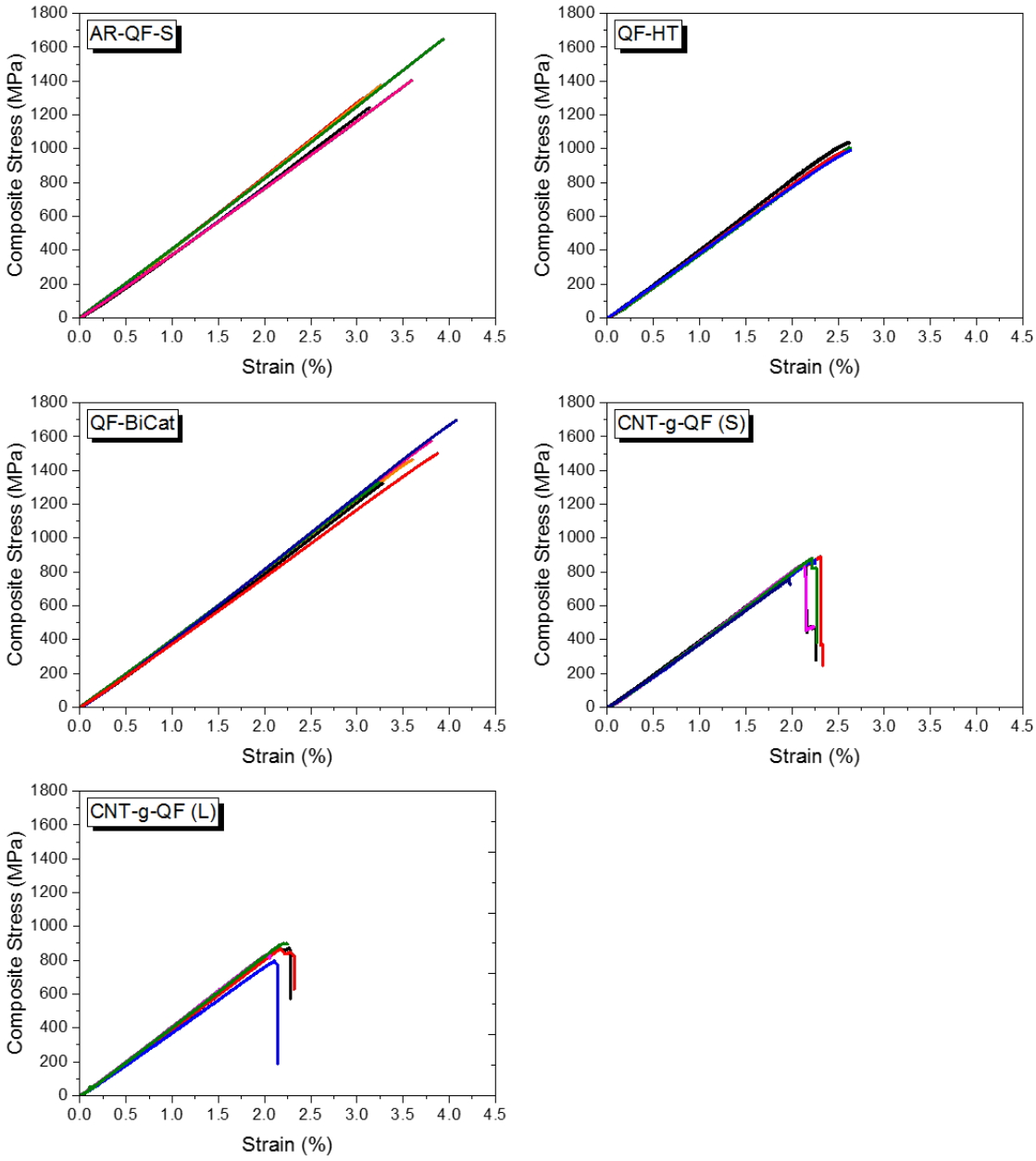

Fig. S13. Collated tensile data for all bundle composites.

Table S2. Additional mechanical properties for the set of UD bundle composites calculated using volume fraction to determine effective QF properties with standard error associated.

	Eff. fibre strength (GPa)	**Eff. fibre Young's modulus** (GPa)	**UD Composite Fibre volume fraction** (%)	**# of spec.**
AR-QF-S	2.83 ± 0.11	79.5 ± 1.4	32.1 ± 1.2	6
QF-HT	2.04 ± 0.02	79.0 ± 0.9	33.6 ± 1.2	4
QF-BiCat	3.02 ± 0.11	79.2 ± 0.6	32.5 ± 1.2	6
CNT-g-QF (S)	1.74 ± 0.04	79.2 ± 0.6	33.0 ± 1.1	6
CNT-g-QF (L)	1.74 ± 0.03	80.9 ± 1.1	32.6 ± 1.8	5

S9 Single fibre pull-out test

Table S3. Single fibre pull-out test results with interfacial shear strength (IFSS) determined using fibre diameter after pull-out with standard error associated. Embedded area shown in **Fig. S14**.

	IFSS (MPa)	**Fibre diameter after pull-out** (μm)	**# of spec.**
AR-QF-S	80.9 ± 1.7	13.0 ± 0.2	16
QF-HT	70.3 ± 4.5	13.1 ± 0.1	14
QF-BiCat	55.3 ± 0.9	13.2 ± 0.1	22
CNT-g-QF (S)	90.3 ± 2.1	13.0 ± 0.1	16
CNT-g-QF (L)	79.2 ± 2.2	13.2 ± 0.2	17

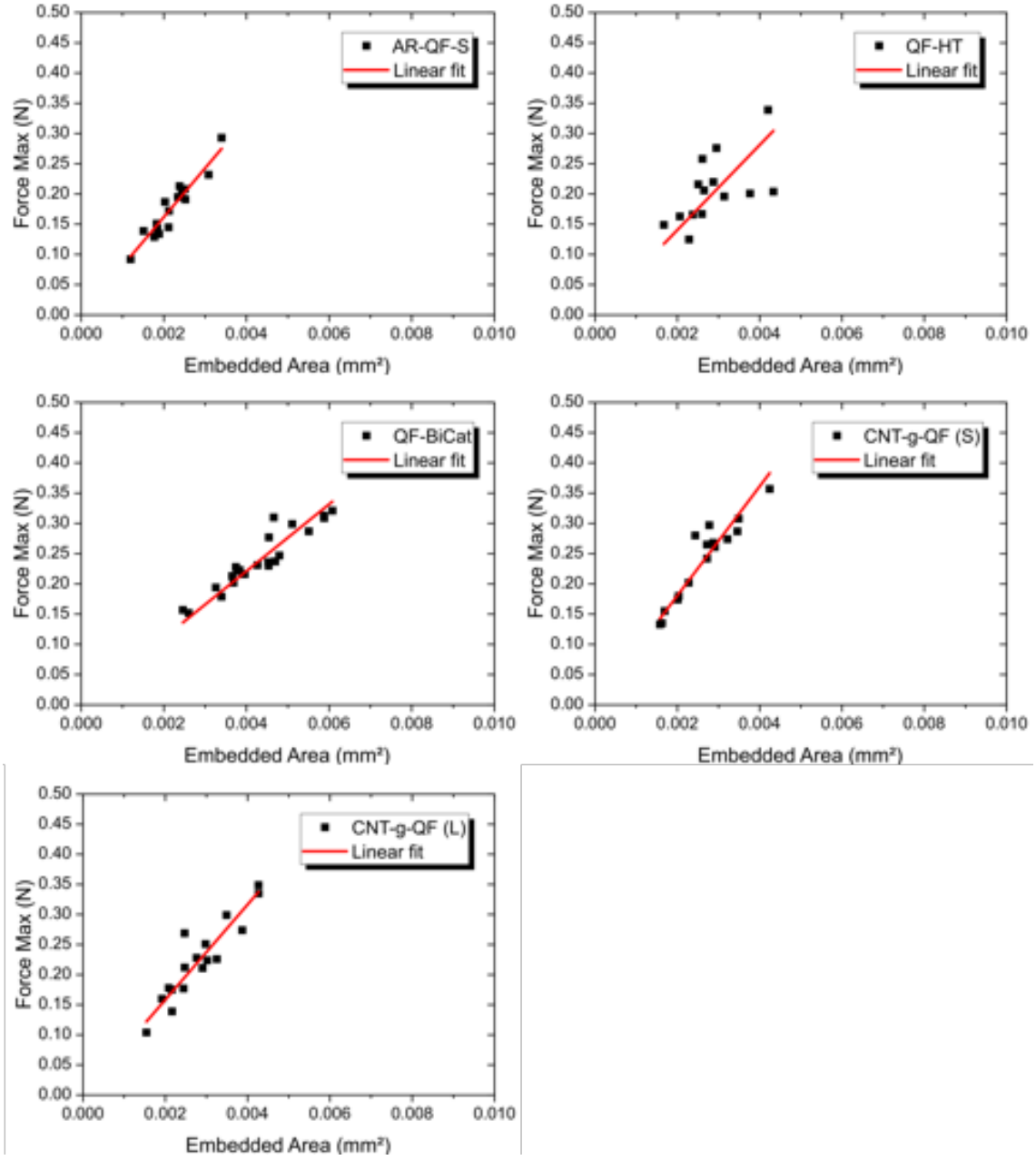

Fig. S14. Collated single fibre pull-out data including linear fits. The slope of the fits corresponds to the apparent IFSS tabulated in **Table S3**.

Acronyms and symbols

A_e, Embedded fibre area; AE, Acoustic emission; AR-QF-S, As-received sized quartz fibre; CF, Carbon fibre; CNT, Carbon nanotube; CNT-g-QF, Carbon nanotube grafted quartz fibre; CNT-g-QF (L), Long carbon nanotube grafted quartz fibre; CNT-g-QF (S), Short carbon nanotube grafted quartz fibre; CVD, Chemical vapour deposition; d_f, fibre diameter; EtOH, Ethanol; F_{max}, Peak pull-out force; GFRP, Glass fibre-reinforced polymer; l_e, Embedded length; I_D, Intensity D-mode; I_G, Intensity G-mode; QF, Quartz fibres; QF-BiCat, Bi-catalyst precursor deposited quartz fibre; QF-HT, Thermally desized quartz fibre; R_0, Initial electrical resistance; ΔR, Electrical resistance variation; SEM, Scanning electron micrographs; τ_{app}, IFSS, Interfacial shear strength; TGA, Thermal gravimetric analysis; UD, Unidirectional.

References

[1] J. Sumfleth, et al., A Comparative Study of the Electrical and Mechanical Properties of Epoxy Nanocomposites Reinforced by Cvd- and Arc-Grown Multi-Wall Carbon Nanotubes, Compos Sci Technol 70(1) (2010) 173-180. https://doi.org/10.1016/j.compscitech.2009.10.007

[2] Saint-Gobain Quartz, Quartzel® Fused Quartz Textiles, 2007, p. 24.

[3] B.L. Wardle, et al., Fabrication and Characterization of Ultrahigh-Volume- Fraction Aligned Carbon Nanotube-Polymer Composites, Adv Mater 20(14) (2008) 2707-14. https://doi.org/10.1002/adma.200800295

[4] R. Gutkin, et al., On Acoustic Emission for Failure Investigation in Cfrp: Pattern Recognition and Peak Frequency Analyses, Mechanical Systems and Signal Processing 25(4) (2011) 1393-1407. https://doi.org/10.1016/j.ymssp.2010.11.014